Available online at www.sciencedirect.com
SCIENCE DIRECT®
International Journal of Heat and Mass Transfer 47 (2004) 3463–3476
International Journal of HEAT and MASS TRANSFER
www.elsevier.com/locate/ijhmt

Numerical study of the enhancement produced in absorption processes using surfactants

J. Castro *, L. Leal, C.D. Pérez-Segarra, P. Pozo

Heat and Mass Transfer Technological Center (CTTC), Universitat Politecnica de Catalunya (UPC), ETSEIT, Colom 11, 08222 Terrassa (Barcelona), Spain

Received 3 June 2003; received in revised form 9 January 2004
Available online 9 April 2004

Abstract

A model that considers the Navier–Stokes equations is used to study the influence of surfactants, substances that improve heat and mass transfer in absorption machines due to Marangoni effect. For solving the free surface location a surface tracking method is used, and for the calculation of surface tension forces, a continuum surface forces model is employed. The coupled equations are solved using the SIMPLEC procedure. Two common surfactants for LiBr aqueous solutions, 1-octanol and 2-ethyl-1-hexanol, are numerically tested and the absorption enhancement produced in a stagnant pool is compared with other researchers' results. For falling film absorption some other results are showed.

PACS: 02.30.Jr; 02.70.Fj; 44.30+v; 47.20.Dr; 68.10−m; 68.15.+e
Keywords: Absorption; Falling film; Refrigeration; Free surface; LiBr; Surfactants; 2-Ethyl-1-hexanol; 1-octanol; Navier–stokes; VOF; CSF

1. Introduction

The reduction of size of heat exchangers that compose absorption chillers is one of the main objectives in order to increase their competitiveness in the air-conditioning market, where the pair water–lithium bromide is used. The prediction of absorption of vapour in falling liquid films processes results very important for the optimisation and reduction of the absorber, the most critical heat exchanger because of its low heat and mass transfer coefficients. Thus, the reduction of the absorber's size is an aspect of prime importance, especially for low power machines. The classical models based on the resolution of boundary layer equations are able to predict reasonably the vapour absorption in liquid falling films in smooth walls [1,2], but the working conditions in real absorption machines, where different techniques of absorption enhancement are implemented, are quite different. These techniques introduce movements in the liquid and vapour phases perpendicular to interface that boundary layer equations cannot simulate.

There are mainly two passive methods of improving the absorption processes. A first method consists on the use of complex surfaces for the heat and mass exchange, e.g. finned tubes [3]. These surfaces increase the exchange area as well as improve the mixing of refrigerant into the solution. The second method employed consists on the use of surfactants. These substances cause gradients of surface tension in the water–LiBr solution, and these gradients induce additional liquid movements at the interface called Marangoni convection [4]. The movement of the liquid falling film also decreases the resistance to heat and mass transfer between the liquid and vapour phases.

Mainly two mechanisms have been proposed for explaining the surface tension gradients: (i) the existence of surfactant 'islands' not dissolved in the interface

* Corresponding author.
E-mail addresses: jesus@labtie.mmt.upc.es (J. Castro), luis@labtie.mmt.upc.es (L. Leal), segarra@labtie.mmt.upc.es (C.D. Pérez-Segarra), pablo@labtie.mmt.upc.es (P. Pozo).
URL: http://www.cttc.upc.edu.

0017-9310/$ - see front matter
doi:10.1016/j.ijheatmasstransfer.2004.01.012

Nomenclature

c	LiBr concentration
C_p	heat capacity at constant pressure
D	mass diffusivity
f	momentum source term
F	volume of fluid
F_{sv}	volumetric surface tension forces
g	gravity
h	height
H	phase change heat
$\dot{m}$	mass flowrate
$\hat{n}$	unitary vector normal to interface
p	pressure
Re	Reynolds number
$\hat{s}$	unitary vector tangential to interface
S	heat source term
t	temperature
u	velocity in horizontal direction
v	velocity in vertical direction
$\vec{V}$	velocity vector
w	width
x	horizontal coordinate
y	vertical coordinate

Greek symbols

β, β^+	thermal and concentration change volumetric expansion coefficients
ϕ	generic physical property
Γ	mass flowrate per unit length
κ	interface curvature
λ	thermal conductivity
μ	dynamic viscosity
ρ	density
σ	surface tension
τ	time

Subscripts and superscripts

0	value at previous time period
a	absorption
H_2O	water
in	inlet
it	interface
LiBr	lithium bromide
l	liquid
r	reference
out	outlet
v	vapour
w	wall

liquid–vapour [4]; (ii) the presence of surfactant at the interface caused by the 'salting out' mechanism [5,6]. This second mechanism appears to be the explanation for the absorption improvements with surfactant concentrations under the solubility limit, when the surfactant 'islands' cannot be formed. Daiguji et al. [6] employed the 'salting out' model for simulating the water vapour absorption in a stagnant pool of LiBr under the solubility limit of surfactant. Their results, reproduced in a previous work [7], indicate that in the case of the strongest enhancements of the absorption rates caused by interface movements, the experimental values do not agree well with the results of the numerical calculation. Many reasons could explain the difference between theoretical and experimental values like limitations of the numerical model employed, interfacial phenomena related to the Marangoni instability not well explained by the 'salting out' effect, especially in cases where the departure from equilibrium is large or the concentration of surfactant exceeds the solubility limit [6].

Very few approaches have been done in solving the Navier–Stokes equations in absorption processes. In [8] Hozawa et al. simulated the absorption process in a stagnant pool. In a later work Daiguji et al. [6], made a comparison between numerical and experimental results of absorption also in a stagnant pool for 1-octanol and 2-ethyl-1-hexanol taking into account the surface tension derivative measurements with respect to temperature and LiBr concentration under static conditions. In other work Koenig et al. [9] gave numerical results also for static absorption in a thin film for different Marangoni numbers. On the other hand, Min and Choi [10] applied a numerical model for the resolution of absorption processes over horizontal tubes. In that work, surface tension effects were considered, but not the effects of surface tension derivatives as in the previous reported works.

A model based on the resolution of the Navier–Stokes equations for the liquid and vapour phases was applied at [7] for the resolution of cases of absorption enhancement in falling film solutions produced by surfactant due to the 'salting out' mechanism, where some data of surface tension gradients are known. The free surface flow was solved in a Eulerian mesh, thus the model implemented was based on a surface capturing method. The advection of the density is computed by means of a volume of fluid technique (VOF) [11] and the surface tension forces are modelised and implemented by means of a continuum method (CSF) [12]. The pressure–velocity coupling is solved by means of the SIMPLE-family

procedure [13]. The results presented in [7] were not conclusive, due to problems of instability of the numerical algorithm employed when numerical ripples are produced. In a further work [14] some additional results indicated the importance of simulating the vapour phase in the absorption process in a stagnant pool. For falling film absorption processes some demonstrative results were showed, but the CPU time required for these calculations and problems on numerical stability in some free surface configurations did not allow many numerical studies. The stability of the code has been improved and the cases presented at [14] have been completed, reporting here some additional results.

2. Mathematical formulation and resolution

The governing equations of the model used are:

$$\frac{\partial \rho}{\partial \tau}+\frac{\partial \rho u}{\partial x}+\frac{\partial \rho v}{\partial y}=0 \tag{1}$$

$$\frac{\partial \rho u}{\partial \tau}+\frac{\partial \rho uu}{\partial x}+\frac{\partial \rho vu}{\partial y} = -\frac{\partial p}{\partial x}+\frac{\partial}{\partial x}\left(2\mu\frac{\partial u}{\partial x}\right)+\frac{\partial}{\partial y}\left(\mu\frac{\partial v}{\partial x}+\mu\frac{\partial u}{\partial y}\right)+f_x \tag{2}$$

$$\frac{\partial \rho v}{\partial \tau}+\frac{\partial \rho uv}{\partial x}+\frac{\partial \rho vv}{\partial y} = -\frac{\partial p}{\partial y}+\frac{\partial}{\partial y}\left(2\mu\frac{\partial v}{\partial y}\right)+\frac{\partial}{\partial x}\left(\mu\frac{\partial u}{\partial y}+\mu\frac{\partial v}{\partial x}\right)+f_y \tag{3}$$

$$\frac{\partial \rho C_p t}{\partial \tau}+\frac{\partial \rho u C_p t}{\partial x}+\frac{\partial \rho v C_p t}{\partial y} = \frac{\partial}{\partial x}\left(\lambda\frac{\partial t}{\partial x}\right)+\frac{\partial}{\partial y}\left(\lambda\frac{\partial t}{\partial y}\right)+S \tag{4}$$

$$\frac{\partial c}{\partial \tau}+u\frac{\partial c}{\partial x}+v\frac{\partial c}{\partial y}=D\left(\frac{\partial^2 c}{\partial x^2}+\frac{\partial^2 c}{\partial y^2}\right) \tag{5}$$

$$\frac{\partial F}{\partial \tau}+u\frac{\partial F}{\partial x}+v\frac{\partial F}{\partial y}=0 \tag{6}$$

where (1) is the mass conservation, (2) and (3) the x and y components of momentum conservation, respectively, (4) the energy conservation, (5) the conservation of the non-volatile absorbent (in this case LiBr) and (6) the volume of fluid conservation equation. It has to be indicated that in this equation the exchange of mass between phases due to the absorption processes is neglected in Eq. (6) because of the low mass transfer rates. Another observation to be done is that for the mass species equation only liquid phase is considered, with constant fluid properties including mass diffusivity.

The source term of Eqs. (2) and (3) are divided in gravity forces and volumetric surface tension forces:

$$f_x=\rho g_x[1+\beta(T-T_r)+\beta^+(c-c_r)]+F_{svx} \tag{7}$$

$$f_y=\rho g_y[1+\beta(T-T_r)+\beta^+(c-c_r)]+F_{svy} \tag{8}$$

The normal and tangential stresses at the interface are incorporated to the momentum equations by the consideration of variable properties in function of F. However, the balance of forces at the free surface is presented here for easy understanding:

$$p_l-p_v+\sigma\kappa=2\mu_l\left(\hat{n}_x\frac{\partial u}{\partial n}+\hat{n}_y\frac{\partial v}{\partial n}\right)_l-2\mu_v\left(\hat{n}_x\frac{\partial u}{\partial n}+\hat{n}_y\frac{\partial v}{\partial n}\right)_v \tag{9}$$

for the normal direction at the interface, where $\hat{n}_x$ and $\hat{n}_y$ are the x and y components of the unitary normal vector to the interface, and:

$$\mu_v\left(\hat{s}_x\frac{\partial u}{\partial n}+\hat{n}_y\frac{\partial v}{\partial s}+\hat{n}_x\frac{\partial u}{\partial s}+\hat{s}_y\frac{\partial v}{\partial n}\right)_v -\mu_l\left(\hat{s}_x\frac{\partial u}{\partial n}+\hat{n}_y\frac{\partial v}{\partial s}+\hat{n}_x\frac{\partial u}{\partial s}+\hat{s}_y\frac{\partial v}{\partial n}\right)_l=\frac{\partial \sigma}{\partial s} \tag{10}$$

for the tangential direction, where $\hat{s}_x$ and $\hat{s}_y$ are the x and y components of the unitary tangential vector to the interface. The surface and normal derivatives are, respectively:

$$\frac{\partial}{\partial s}=\hat{s}\cdot\vec{\nabla},\quad \frac{\partial}{\partial n}=\hat{n}\cdot\vec{\nabla} \tag{11}$$

Eq. (9) is the balance of the superficial forces in the normal direction to the interface, and Eq. (10) expresses the balance of the superficial forces in the tangential direction. In the latter, the surface tension variation due to temperature and LiBr concentrations gradients plays an important role. Due to the absorption process, the boundary conditions at the interface for the conservation of energy and conservation of LiBr equations are (12) and (13):

$$\lambda_l\frac{\partial t}{\partial n}-\lambda_v\frac{\partial t}{\partial n}=-H_a\frac{D\rho}{c_{it}}\frac{\partial c}{\partial n} \tag{12}$$

$$t_{it}=f(c_{it},p_{it}) \tag{13}$$

Eq. (12) expresses the interface heat balance where the heat due to the phase change is considered. Eq. (13) relates the temperature and the LiBr concentration under the hypothesis of equilibrium. This expression has been extracted from [15] for the calculations. The deduction of the mass absorbed in Eq. (12) for mobile interfaces (Fig. 1) proceeds as follows: the flow of mass absorbed as far as vapour and liquid is concerned can be expressed as the difference between the velocity of the fluid normal to the interface and the velocity of the interface, multiplied by the density of the liquid—that is, the water–LiBr solution—(14), on the one hand, and the density of the water vapour (15) on the other hand:

$$\dot{m}_a=\rho_l(\vec{V}_l-\vec{V}_{it})\cdot\hat{n} \tag{14}$$

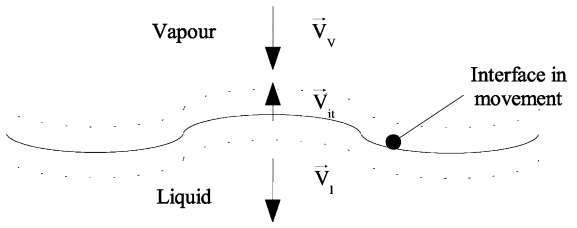

Fig. 1. Absorption process at the interface.

$$\rho_v(\vec{V}_v - \vec{V}_{it}) \cdot \hat{n} = \rho_l(\vec{V}_l - \vec{V}_{it}) \cdot \hat{n} \tag{15}$$

If the right side of expression (15) is developed, the whole flow of water–LiBr solution is divided between the flow of water and the flow of LiBr (16):

$$\rho_l(\vec{V}_l - \vec{V}_{it}) \cdot \hat{n} = \rho_{l,H_2O}(\vec{V}_{l,H_2O} - \vec{V}_{it}) \cdot \hat{n} + \underline{\rho_{l,LiBr}(\vec{V}_{l,LiBr} - \vec{V}_{it}) \cdot \hat{n}} \tag{16}$$

The flow of LiBr towards the interface is zero (underlined term of Eq. (16)), because it is not volatile:

$$\rho_l(\vec{V}_l - \vec{V}_{it}) \cdot \hat{n} = \rho_{l,H_2O}(\vec{V}_{l,H_2O} - \vec{V}_{it}) \cdot \hat{n} = \rho_{l,H_2O}\vec{V}_{l,H_2O} \cdot \hat{n} - \rho_{l,H_2O}\vec{V}_{it} \cdot \hat{n} \tag{17}$$

For the water flow, developing the expression and applying Fick's Law, the following expression results (18):

$$\rho_l(\vec{V}_l - \vec{V}_{it}) \cdot \hat{n} = -\rho_l D\frac{\partial(1-c)}{\partial n} + \rho_l(1-c_{it})\vec{V}_l \cdot \hat{n} - \rho_{l,H_2O}\vec{V}_{it} \cdot \hat{n} \tag{18}$$

Adding and subtracting $\rho_{l,H_2O}\vec{V}_{it}$ in Eq. (18) and rearranging the expression, it can be seen a term proportional to the concentration derivative, another term that is the mass flow absorbed multiplied by the water mass fraction, and a last term where the interface velocity is involved. This last term (underlined below) results zero, for the definition of partial density of substance:

$$\rho_l(\vec{V}_l, -\vec{V}_{it}) \cdot \hat{n} = -\rho_l D\frac{\partial(1-c)}{\partial n} + \rho_l(1-c_{it})(\vec{V}_l - \vec{V}_{it}) \cdot \hat{n} - \underline{\vec{V}_{it}(\rho_l(1-c_{it}) - \rho_{l,H_2O}) \cdot \hat{n}} \tag{19}$$

Thus, it can be operated the whole expression and find that the flow of mass absorbed is proportional to the mass flow due to molecular diffusivity in the LiBr solution (20):

$$\dot{m}_a = \rho_l(\vec{V}_l, -\vec{V}_{it}) \cdot \hat{n} = \frac{\rho_l D}{c_{it}}\frac{\partial c}{\partial n} \tag{20}$$

The coupling between pressure and velocities is solved with a segregated algorithm of the SIMPLE-family [13] (SIMPLEC) using staggered grids for the velocities. The incompressibility condition is applied by means of a 'volume continuity equation' [16] in order to apply the same equation for the whole domain. Concerning to the volume of fluid equation, the interface tracking algorithm based on the piecewise constant/stairstepped VOF method proposed by Hirt and Nichols [11] is used to reduce the numerical smearing of the variable F.

The physical properties (density, viscosity, thermal conductivity and heat capacity) are ponderated according to the value of the volume of fluid function as in expression (21):

$$\phi = \phi_l F + \phi_v(1-F) \tag{21}$$

The diffusion fluxes (heat conduction, viscous stresses) are computed by means of the harmonic mean method [13] that ensures the continuity of these fluxes across the interface.

For the calculation of surface tension forces, heat of absorption and mass absorbed, a continuum method is employed (CSF) [12]. This technique interprets a surface boundary condition as a continuous two-dimensional effect only active in the interface zone, where there are gradients of the volume of fluid function F. So, the surface tension forces are converted into forces per unit volume (F_{sv}) [17,18], and the heat of absorption into a volumetric heat source (source term of Eq. (4)). Both are calculated from the normal vectors at the free surface. For the calculation of normal vectors, the ALE-like scheme [12] (indirect differentiation to the unit normal) has been adopted.

3. Results

3.1. Absorption in a stagnant pool

A situation of absorption in a stagnant pool improved by surfactants has been taken as benchmark for the comparison between numerical calculations and experimental results. The situation reported by Daiguji et al. [6] (see Fig. 2) has been reproduced. The main difference between the numerical model in [6] is that the one presented here considers as well the movements of the vapour phase, so it gives more information about flow configuration. However, it is necessary more CPU time for computing the vapour phase, due mainly to its higher sensitivity to surface tension effects due to its lower density.

The LiBr solution is placed in an adiabatic pool in such conditions that its equilibrium pressure is lower than the one existing in the vapour, so the absorption is produced. The boundary conditions taken for the simulation for the vapour phase are zero derivative for all variables: velocities, pressure and temperature. Obviously, the equation of conservation of LiBr is not considered in the vapour phase. In this case, the vertical velocity at the interface is considered as zero (the water velocity value at the interface is negligible), and no

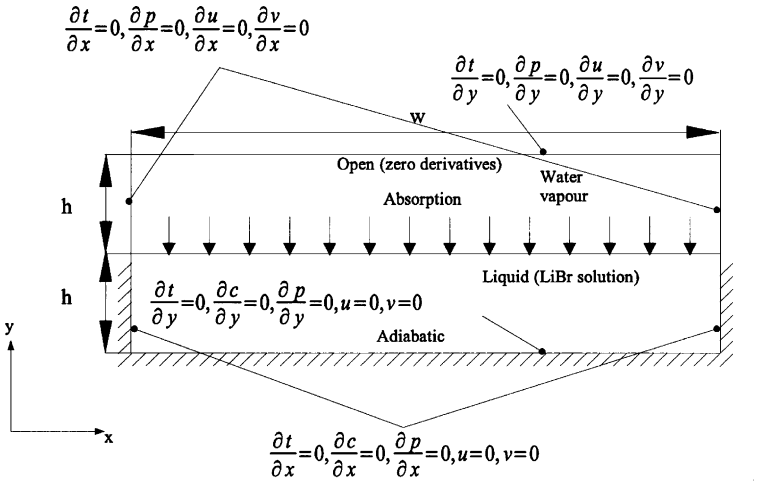

Fig. 2. Physical domain of the pool and boundary conditions.

Table 1
Physical properties and parameters used for the stagnant pool case

h	0.010 m	λ_l	4.38×10^{-1} W/(m K)	λ_2	1.796×10^{-2} W/(m K)
l	0.076 m	D_l	1.43×10^{-9} m^2/s	D_v	0.0 m^2/s
$\Delta\tau_0$	10^{-8} s	μ_l	3.83×10^{-3} Pa s	μ_v	9.735×10^{-5} Pa s
p	2315 Pa	ρ_l	1624 kg/m^3	ρ_v	1.7195×10^{-2} kg/m^3
t_0	303 K	β_l	3.645×10^{-4} K^{-1}	β_v	3.4112×10^{-3} K^{-1}
c_0	55.22 wt.%	β_l^+	-1.109×10^{-1} wt.%$^{-1}$	β_v^+	0.0 wt.%$^{-1}$
H_a	2568 kJ/kg	C_{pl}	2184 kJ/(kg K)	C_{pv}	1865 kJ/(kg K)
$\partial\sigma/\partial t$	-2.1×10^{-4} N/(m K)	$\partial\sigma/\partial c$	-6.4×10^{-4} N/(m wt.%)	σ	6.0×10^{-2} N/m

movement of the interface is considered. The physical properties and parameters of the simulation are given in Table 1. It has to be indicated that a variable time increment for the transient calculation has been used in order to optimise the CPU time. The difference between the case simulated here and the one done by Daiguji is that the vapour phase is also considered in this study together with the liquid phase.

In order to generate the cellular convection, a local variation of LiBr concentration is given at $x = l/2$, for $\tau = 0.1$ s. The data to be compared is the amount of water vapour absorbed as function of time. This amount of absorbed water increases until reaching a value of equilibrium in which it stabilises. The surfactant used is *n*-octanol with a concentration of 25 ppm. The mesh used by Daiguji is $n = 42$ (for liquid phase only, vertical) $\times$ $m = 78$ (horizontal) points vertically concentrated towards the interface. In the baseline case ($n = 42$), the same mesh is used for the vapour phase, but more simulations with a coarse ($n = 21 \times 2$, $m = 39$, Fig. 3) and refined ($n = 84 \times 2$, $m = 156$ and $n = 168 \times 2$, $m = 312$, Fig. 4) meshes have been carried out in order to find a solution closer to the numerical asymptotic one.

The simulations carried out with the calculation of the vapur phase agree better with the experimental data reported by Daiguji et al. [6] where only considers the liquid phase. These results reinforces the 'salting out' mechanism as explanation for the absorption enhancement when surfactant concentration is under its solubility limit and it also indicates the importance of the movements in the vapour phase in the absorption mechanism. In order to confirm that, a last simulation

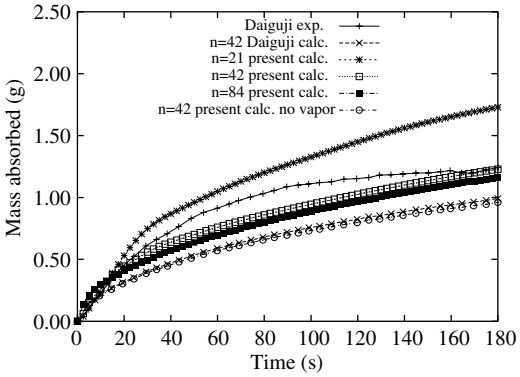

Fig. 3. Comparison between experimental and numerical results given by the model.

has been performed only taking into account the liquid, and the results obtained are quite similar to the calculated ones reported in [6] and even calculated the mass absorbed is sligthly lower.

In the case of the most refined mesh ($n = 168 \times 2$) the calculation has not been completed in the whole time period due to the excessive required CPU time for the calculations (Fig. 4). It can be observed that the solutions given by the two most refined meshes ($n = 84$ and 168) are very close, so these two solutions are very close to the numerical asymptotic one. Due to its influence, the vapour phase is always considered for the calculations in falling film flow in the next section.

Another comparison has been done between the numerical results given by the model and the ones reported by Daiguji et al. [6]. In this case the baseline mesh ($n = 42$) has been taken and the study has been done for three different depths: 10, 7 and 4 mm. The results are showed in Figs. 5–7. In these cases the same conditions of calculation are maintained.

There are four results for each depth of the pool: the experimental and numerical results reported by Daiguji et al. [6] with 1-octanol 25 ppm, the experimental data also reported by Daiguji et al. [6] without surfactant and

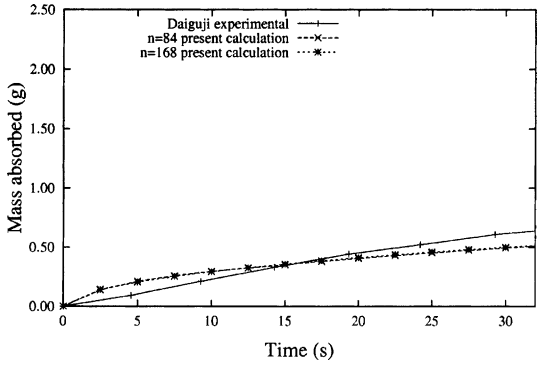

Fig. 4. Comparison between the two refined meshes.

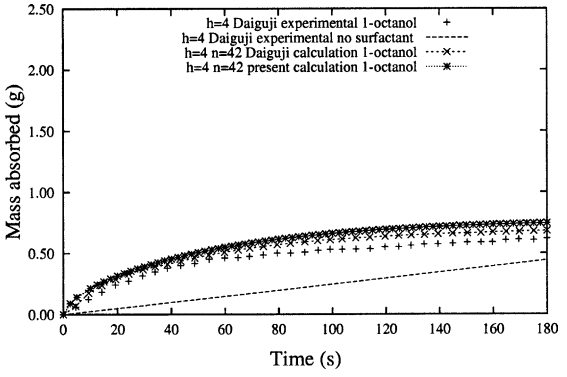

Fig. 5. Comparison for depth $h = 4$ mm.

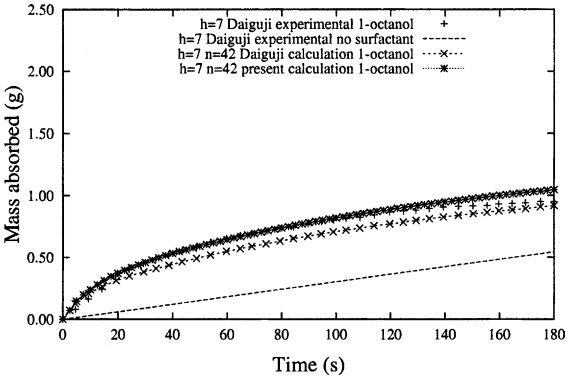

Fig. 6. Comparison for depth $h = 7$ mm.

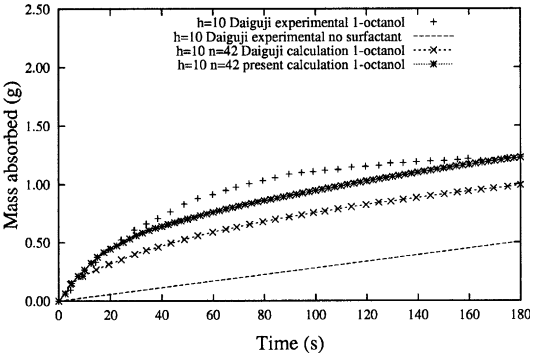

Fig. 7. Comparison for depth $h = 10$ mm.

finally the numerical results calculated in this work with vapour phase. From these, it can be observed that the results obtained by the numerical model with the vapour phase also agree better with the experiment than the results reported by Daiguji for the higher depths (10 and 7 mm). However, the agreement is lower at the lowest depth (4 mm). From a qualitative point of view, at lower values of depth the enhancement is less important. This result suggests that the mixing of water absorbed is improved when the Marangoni convection cells are more important, and those are more important when depth is higher.

A last comparison has been done with another well known surfactant, 2-ethyl-1-hexanol. In this case a concentration of 25 ppm has been considered. The values of $\partial\sigma/\partial t$ and $\partial\sigma/\partial c$ chosen for the calculations are respectively: -2.1×10^{-4} N/(m K) and -1.5×10^{-3} N/(m wt.%) [6].

Fig. 8 shows a graphical comparison between the experimental and numerical values of Daiguji et al. [6] and the present calculation. As in the previous cases, the results performed with the vapour phase agree better with the experimental data than the numerical results without vapour phase.

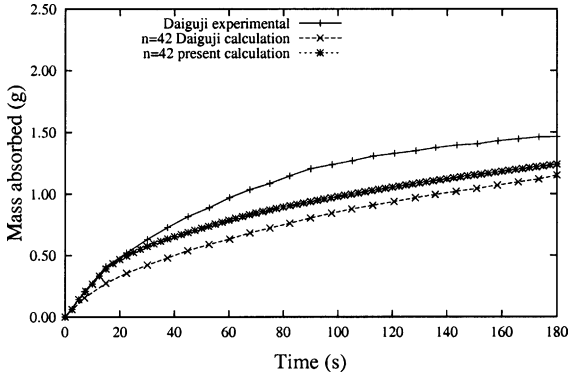

Fig. 8. Comparison for 2-ethyl-1-hexanol (25 ppm).

Next Fig. 9 shows the evolution of the absorption process by means of different plots of temperatures, LiBr concentrations and streamlines, for the case of 1-octanol and 10 mm of depth (mesh used, $n = 42 \times 2$). It can be observed in the streamlines that at the beginning the movements start at the center of the interface, where the perturbation is introduced. Then, the Marangoni cells are produced both in the liquid and vapour phase, being more pronounced in the vapour phase, due to its lower density. Finally, the last plots show the formation in the liquid phase of other cells due to gravity forces that become more important when the temperature and LiBr concentration gradients inside the liquid are significant. These movements are reflected in the plot of temperatures and concentrations: the lines are not parallel to the horizontal line, reflecting the formation of vortices in the liquid phase.

3.2. Falling film absorption

In this section the model will be tested in falling film regime in a vertical wall. Although falling film absorption is a situation of industrial interest, it has not been possible to reproduce an experiment due to high computational time needed for the calculations. So, the domain dimensions and time simulated have been limited and, by consequence, a direct comparison is not available for the moment. However, in case of doing a comparison with experimental data it has to be remarked that it is necessary to achieve a total wetted area of the absorber surface for all cases reproduced, in order to discard the improvements due to the enhancement of the wetted area of the heat and mass transfer surface. For this reason, not all the available information in the literature is valid.

Fig. 10 shows the physical domain and the boundary conditions used for falling film absorption. The initial value of velocities corresponds to Nusselt's parabolic solution in the liquid phase. In the vapour phase a linear velocity profile is adopted. With respect to the temperature and LiBr concentration, the initial values are the same in all domain of calculation as the inlet values. At the wall the temperature value is fixed at 38 °C. This value has been considered as realistic for air-cooled absorbers. Although the movements in the transversal direction to the plane considered in the calculation can

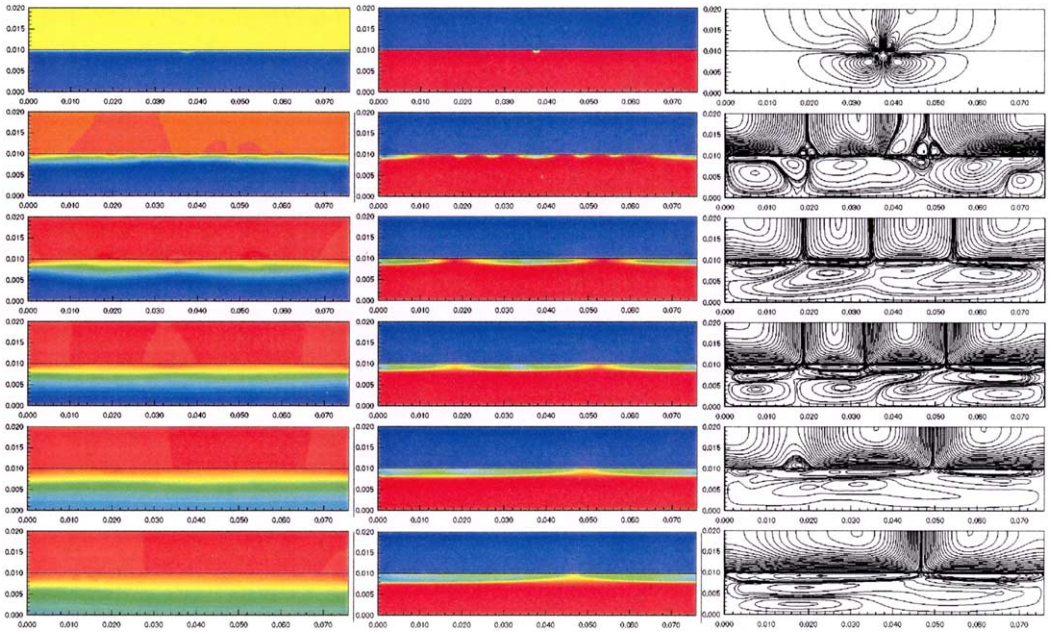

Fig. 9. Temperatures, LiBr concentrations and streamlines at 1, 10, 30, 60, 120 and 180 s (from up to down).

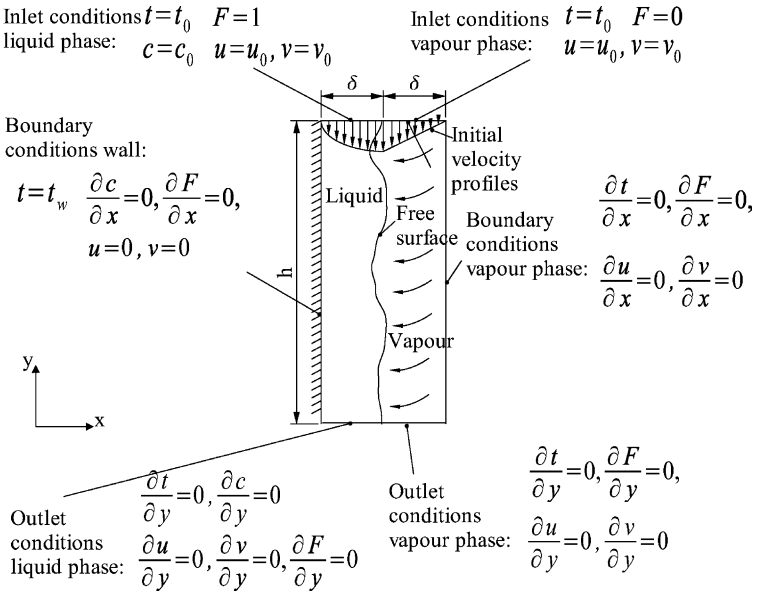

Fig. 10. Physical domain of the falling film and boundary conditions.

Table 2
Physical properties and parameters used for the baseline case

h	2.0 mm	λ_l	0.438 W/m K	λ_v	0.078 W/m K
δ	0.24 mm	μ_l	4.7×10^{-3} Pa s	μ_v	1.0×10^{-5} Pa s
$\Delta\tau$	Variable	D_l	1.4×10^{-9} m^2/s	D_v	0
p	1138 Pa	ρ_l	1624 kg/m^3	ρ_v	0.009 kg/m^3
t_{in}	312.27 K	Cp_l	2200 kJ/kg K	Cp_v	1864 kJ/kg K
t_w	311.15 K	β_l	3.6×10^{-4} K^{-1}	β_v	3.4×10^{-3} K^{-1}
c_{in}	57.00 wt.%	β_l^+	−0.11 wt.%$^{-1}$	β_v^+	0

Table 3
LiBr solution surface tension values for different surfactants

Surfactant	σ (N/m)	$\partial\sigma/\partial t$ (N/m K)	$\partial\sigma/\partial c$ (N/m wt.%)
No surfactant	0.080	-1.0×10^{-4}	3.8×10^{-4}
1-Octanol (25 ppm)	0.026	-2.1×10^{-4}	-6.4×10^{-4}
2-Ethyl-1-hexanol (30 ppm)	0.064	7.3×10^{-4}	-1.3×10^{-3}

be important in the absorption enhancement, the simulations have been limited to two-dimensional calculation mainly to CPU time limitations. Without a comparison between two and three dimensional calculations it is difficult to evaluate the influence of these movements in transversal direction. However, the concentration and temperature gradients in the vertical direction are more important, due to the boundary conditions.

Table 2 shows the physical properties and geometry employed for the case simulated. The value of δ corresponds to a value of mass flow about 103.5 kg/(m h) ($Re = 4^*\Gamma/\mu = 25$), a typical value for absorption machines. The value of δ varies according to the Reynolds number. It is important to stand out the limited physical domain due to the high CPU time required for the calculations.

Table 3 shows the values taken of surface tension and surface tension derivatives with respect to the temperature and LiBr concentration for two common surfactants used in the industry, 1-octanol (25 ppm) and 2-ethyl-1-hexanol (30 ppm). For the 1-octanol, the data taken for the calculation of the surface tension derivatives are the same as the ones used by Daiguji et al. [6] and for the surface tension the data have been extracted from Hozawa et al. [8]. Although in that work there are no data for LiBr concentrations higher than 50%, it has

Table 4
Comparison with three different meshes

Surfactant	Mesh					
	Mass absorbed (kg/(s m) $\times 10^5$)			Heat rejected (W/m)		
	60×50	120×100	240×200	60×50	120×100	240×200
No surfactant	1.1766	1.3190	1.3020	12.201	12.233	12.329
1-Octanol	1.2157	1.4529	1.4808	12.189	12.092	12.306
%Enhancement	3.3	10.1	13.7	−0.1	−1.2	−0.2
2-Ethyl-1-hexanol	1.2713	1.5048	1.5497	12.196	12.050	12.246
%Enhancement	8.0	14.1	19.0	−0.0	−1.5	−0.7

been taken the minimum value of surface tension reported, due to the high LiBr concentration that favours the 'salting out' effect for the 1-octanol. The data for 2-ethyl-1-hexanol have been extracted from Kim et al. [19].

The first study done is the comparison of the results with different meshes to see the dependence with respect to the mesh. Three different meshes have been used ($n°$ of cells in horizontal direction $\times n°$ of cells in vertical direction): 60×50, 120×100, 240×200 all with constant mesh density. Table 4 contains the values of mass absorbed and heat rejected to the wall for the three different cases and the three different meshes.

There are different degrees of absorption enhancement according to the surfactant and mesh used, but the results for the two last meshes are quite similar. As a conclusion of this particular study, it results that an uniform mesh of 120×100 points is enough for assuring results roughly independent from the mesh. The heat rejected does not present significant differences between the different cases.

Fig. 11 shows the evolution of the mass absorbed rates during the time simulated for the different cases. The results are qualitatively similar for the three different curves compared: no surfactant, 1-octanol and 2-ethyl-1-hexanol, with the mesh of 120×100 points. The highest value of mass absorbed corresponds to the beginning, when the LiBr concentration, near the

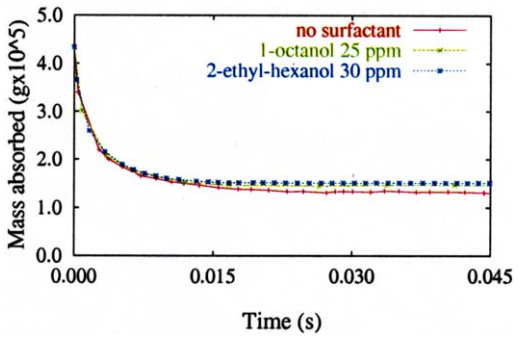

Fig. 11. Mass absorbed vs. time.

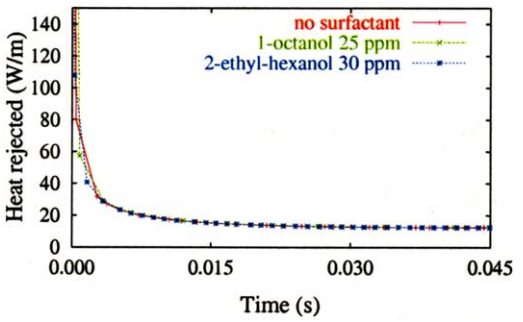

Fig. 12. Heat rejected vs. time.

interface, is higher than the equilibrium one in these conditions. This fact leads to high concentration gradients that are proportional to mass absorbed rates. These absorption rates achieve a value of stability quite faster (in a period of time about 3×10^{-2} s.). However, it can be observed that a completely stable value is not achieved in all cases, so the numerical results reported of mass absorbed and heat rejected are averaged values.

With respect to heat rejected (Fig. 12), there is not significant differences according to the surfactant used. It indicates that the interface thermal boundary layer due to the heat of absorption does not reach the wall in the distance simulated (2 mm).

In order to study the enhancement due to the action of the surfactants several parameters will be modified

Table 5
Enhancement according to falling film length and surfactant

Surfactant	Mass absorbed (kg/(s m)) $\times 10^5$	
	Length (mm)	
	2	4
No surfactant	1.3190	1.9709
1-Octanol	1.4529	2.0788
%Enhancement	10.1	5.5
2-Ethyl-1-hexanol	1.5048	2.1202
%Enhancement	14.1	7.6

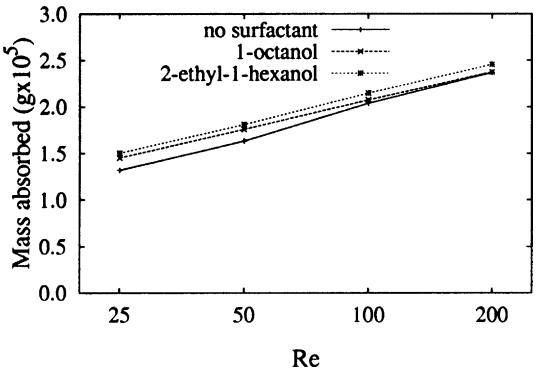

Fig. 13. Mass absorbed vs. *Re*.

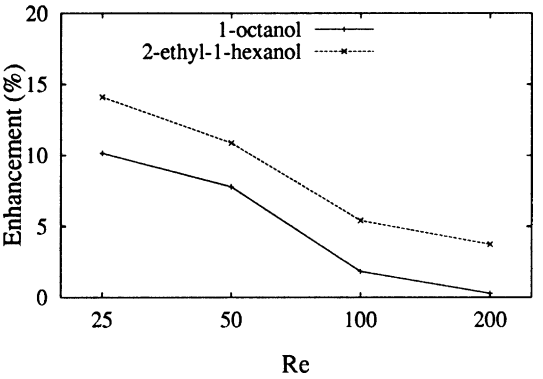

Fig. 14. Enhancement vs. *Re*.

such as: falling film length, Reynolds number and absorption pressure (mass transfer potential).

Table 5 shows the comparison of the absorption improvement computed between two falling film lengths: 2 and 4 mm with $Re = 25$. It can be observed that there is a lower absorption enhancement for 4 mm than for 2 mm for the two surfactants. The boundary conditions for the temperature and LiBr concentration lead to higher gradients at the beginning of the falling film, so higher enhancements are expected for 2 mm than for 4 mm as the results show.

The following plots (Figs. 13 and 14) show the results in case of changing the Reynolds falling film number. On the left side, the mass of water absorbed, and on the right side the absorption ratio enhancement are reported for each case. The two graphics are in logarithmic scale with respect to the Reynolds number. At high Reynolds numbers, the gravity forces dominates the surface tension ones, so the absorption enhancement decreases with *Re* and finally is negligible. 2-ethyl-1-hexanol produces a significant improvement of the mass absorbed, with a maximum value of about 14% at $Re = 25$. On the other hand, the maximum improvement of the mass absorbed for 1-octanol is also about 10% at the same Reynolds value.

A last study has been done for comparing the enhancement produced by the two surfactants at different mass transfer driving potentials. It means that the mass absorbed has been compared at four different absorption pressures: 1051.7, 1138.7, 1225.6 and 1312.6 Pa, maintaining the rest of conditions constant with respect to previous calculations ($Re = 25$ and 2 mm of falling film length). The vapour pressure at initial bulk temperatures (312.27 K and 57% of LiBr) was 964.8 Pa, so the water vapour pressure differences have been respectively: 86.9, 173.8, 260.7 and 347.6 Pa.

The computed results show that the enhancements produced are also dependent on the mass transfer driving potentials. At low pressure differences the relative absorption enhancement is more important due to the fact that the total mass absorbed rates are lower (see Fig. 16). However, in absolute value the absorption enhancements are increasing with the mass transfer potential, as shown in Fig. 15.

In order to see qualitatively the influence of the two surfactants, some additional plots are shown (Fig. 17). In these cases, the horizontal component of the velocity in the middle plane, close to the interface, is represented. This component of the velocity is a clear indicator of the movements at the interface. Three cases are plotted: no surfactant, 1-octanol (25 ppm) and 2-ethyl-1-hexanol

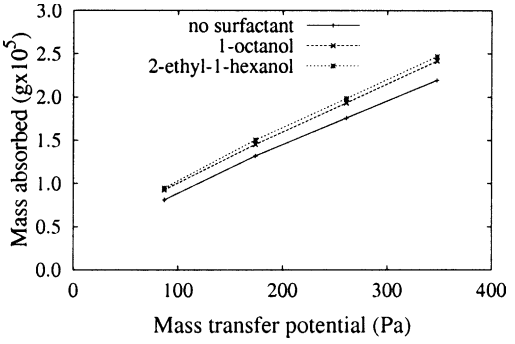

Fig. 15. Mass absorbed vs. mass transfer potential.

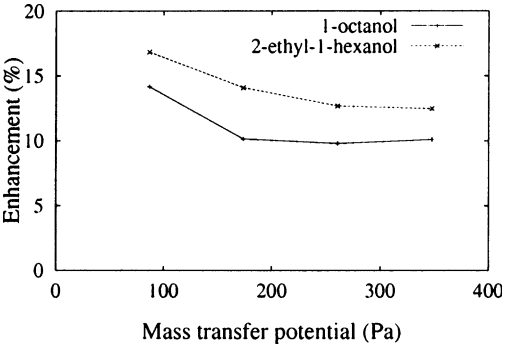

Fig. 16. Enhancement vs. mass transfer potential.

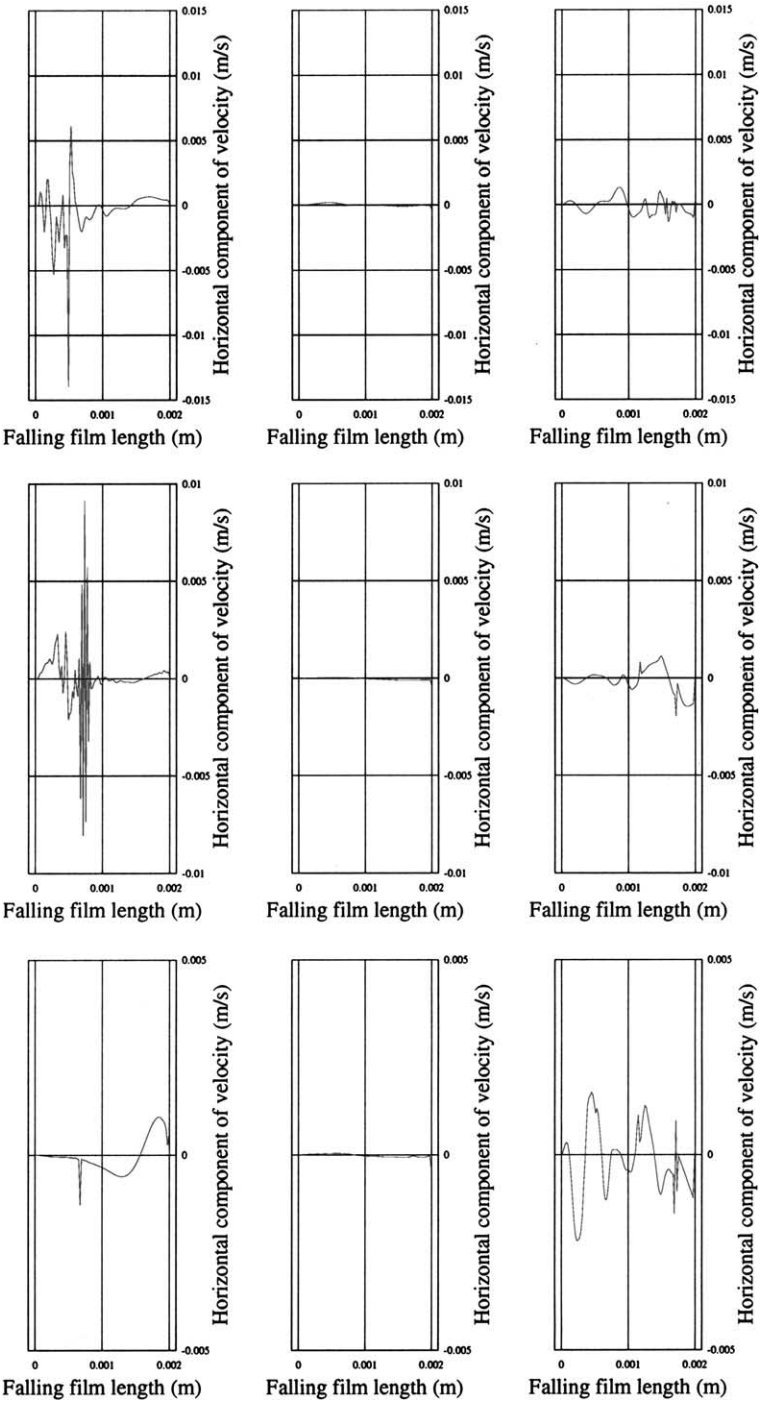

Fig. 17. Horizontal velocities in the middle plane, corresponding to no surfactant, 1-octanol, 2-ethyl-1-hexanol (from left to right), at times 0.015, 0.030 and 0.045 s (from up to down).

(30 ppm). The mesh used is 120×100, with $Re = 25$, 2 mm of falling film length and absorption pressure of 1138.7 Pa.

As expected, the case of the second surfactant, 2-ethyl-1-hexanol, presents the highest values of velocities when the mass absorbed is stabilised ($t = 0.045$ s).

Table 6
Average values and standard deviation of the horizontal velocity at the middle plane, and mass absorbed during three different moments: 0.015, 0.030, 0.045 s

Surfactant	Measurement	0.015 s	0.030 s	0.045 s
No surfactant	Mean velocity (m/s) $\times 10^4$	−3.2850	0.6424	−0.4073
	Standard deviation (m/s) $\times 10^4$	19.3594	18.5918	4.2376
	Mass absorbed (kg/(s m)) $\times 10^5$	1.4149	1.3237	1.2930
1-Octanol	Mean velocity (m/s) $\times 10^4$	0.1496	−0.3241	−0.2180
	Standard deviation (m/s) $\times 10^4$	0.93050	0.60188	0.47642
	Mass absorbed (kg/(s m)) $\times 10^5$	1.4656	1.4330	1.4534
2-Ethyl-1-hexanol	Mean velocity (m/s) $\times 10^4$	−0.9389	−1.3151	−1.7361
	Standard deviation (m/s) $\times 10^4$	6.0366	6.1874	8.6013
	Mass absorbed (kg/(s m)) $\times 10^5$	1.5215	1.5030	1.5044

However, at the beginning the case without surfactant presents the highest values of velocities and, for 1-octanol, the movements are much lower than in the two other cases. In order to analyse the cause of the absorption enhancement for these cases, it is necessary to demonstrate the medium value of this component of the velocity (see Table 6) and the mass absorbed at that moment. This component of velocity favours the mass transfer at the interface, so the mass absorbed. The negative value of the average velocities indicates movement towards the liquid phase.

It can be observed a correlation between the absolute value of the mean velocity (towards the liquid phase) and the mass absorbed, especially for the case of 2-ethyl-1-hexanol. In this case the movements remain almost constant for the time simulated. In the case without surfactant, the movements are much more unstable at the beginning than later, like the movements of a elastic spring (in this case the value of the surface tension is the highest). For 1-octanol, the flow is much more stable (the value of the surface tension is the lowest), and when the flow is stabilised (after 0.030 s) the mean value of the velocity always favours the absorption process.

4. Conclusions

In all cases, there has been observed mass transfer enhancements due to the action of extra surface tension forces. As Daiguji concluded at [6] these results are consistent with the theory of 'salting out', that explains a mechanism of surface tension gradients with surfactant concentrations under the solubility limit. As a consequence, the absorption enhancement would be produced only for fluid (liquid and vapour) movements.

In all situations simulated 2-ethyl-1-hexanol results slightly more efficient than 1-octanol. This fact is coherent with the general impression of the scientific community that 2-ethyl-1-hexanol is a better additive. However, the results reported have to be considered as a preliminary approach. It is important to remark that it is necessary complete information about the values of surface tension of LiBr solution at different absorbent concentrations and temperatures, for different surfactant concentrations under dynamic conditions. Only with these complete data the numerical model will be able to be tested completely vs. experimental data. However, it will be difficult to know if the conditions in which the surface tension is measured were equivalent to the ones produced in dynamic absorption processes.

To overcome these problems, a more detailed model would be necessary for taking into account the adsorption process of the surfactant from the liquid [20] and vapour phases [21] towards the interface and from that, computing the surface tension at each point.

4.1. Absorption in a stagnant pool

An exhaustive comparison has been done in a case of absorption in a stagnant pool between the results obtained with the numerical model presented in this work and the experimental and numerical results of Daiguji et al. [6] in a previous one. From the results obtained, three main conclusions can be remarked:

- From a quantitative point of view, the results obtained by the model, in terms of mass absorbed as function of time, agree better in almost all cases with the empirical results than the ones evaluated with the liquid phase only.
- From a qualitative point of view, the absorption enhancement is more important when the value of surface tension gradients are more important. This was observed in the study of the action of two different surfactants: 1-octanol and 2-ethyl-1-hexanol. The second surfactant (2-ethyl-1-hexanol) produces surface tension gradients higher than 1-octanol and the pool absorbs faster the water vapour with this addi-

tive. Also, the mass absorption enhancements are improved when the depth of the pool is bigger. In those cases the Marangoni cells are more important, so the enhancement is more important.

- However, there are still significant discrepancies between empirical and numerical results. It could be explained by the fact that the simulation carried out is rectangular two-dimensional, not cylindrical in three dimensions as the actual situation. Only a direct comparison with a three-dimensional simulation independent of the mesh could assure the total confidence of this model discarding other effects, like insufficient reposition of surfactant in the adsorption layer at the interface liquid–vapor that would modify the surface tension value measured under static conditions.

4.2. Falling film absorption

After a study of the sensitivity of results with respect to the mesh used to carry out the calculations, different simulations have been done in order to study the absorption enhancement in falling film flow under several conditions: falling film length, Reynolds number and mass transfer potential:

- First of all, different absorption enhancement rates have been found for two different lengths of falling film. When the falling film length is increased from 2 to 4 mm, the rate of absorption enhancement is less important. It can be explained because at the beginning there are more important temperature and LiBr concentration gradients due to the initial boundary conditions.
- When Reynolds number increases, the gravity force dominates the falling film and the effect of the surfactants decreases. By contrary, at low Reynolds numbers, the surface tension forces are dominant and there are more important improvements of the mass absorbed. However, 2-ethyl-1-hexanol is less sensible than 1-octanol when falling film Reynolds number increases because it maintains significant enhancement ratios up to Reynolds values of 100, and 1-octanol only up to 50.
- Finally, for different values of mass transfer potential, the absorption enhancement rates are not constant. These are more important in relative terms at low mass transfer potentials; but in absolute value, the absorption enhancement increases with the mass transfer potential.

Acknowledgements

The research has been financially supported by the 'Ministerio de Ciencia y Tecnologia', Spain (ref. TIC 2003-07970).

References

[1] J.W. Andberg, Absorption of vapours into liquid films flowing over cooled horizontal tubes, Ph.D. thesis, University of Texas, Austin, USA, 1986.
[2] R. Wassenaar, Simultaneous heat and mass transfer in a horizontal tube absorber, Ph.D. thesis, Delft University of Technology, The Netherlands, 1994.
[3] W.A. Miller, H.P. Blanco, Vertical-tube aqueous LiBr falling film absorption using advanced surfaces, in: Proceedings of the International Absorption Heat Pump Conference, vol. 31, ASME, 1993, pp. 185–202.
[4] F. Ziegler, G. Grossman, Review paper: heat transfer enhancement by additives, International Journal of Refrigeration 19 (5) (1996) 301–309.
[5] E. Hihara, T. Saito, Effect of surfactant on falling film absorption, International Journal of Refrigeration 16 (5) (1993) 339–346.
[6] H. Daiguji, E. Hihara, T. Saito, Mechanism of absorption enhancement by surfactant, International Journal of Heat and Mass Transfer 40 (8) (1997) 1743–1752.
[7] J. Castro, C. Oliet, H. Schweiger, A. Oliva, Application of a two-dimensional model for the study of water vapour absorption in falling films of LiBr aqueous solutions with the action of a surfactant, in: Proceedings of the Fourth European Computational Fluid Dynamics Conference (ECCOMAS), vol. 1, Athens, 1998, pp. 286–291.
[8] M. Hozawa, M. Ionue, J. Sato, T. Tsukada, N. Imaishi, Marangoni convection during steam absorption into aqueous LiBr solution with surfactant, Journal of Chemical Engineering of Japan 24 (1991) 209–214.
[9] M.S. Koenig, G. Grossman, K. Gommed, Additive-induced enhancement of heat and mass transfer in a static absorber: a numerical study, in: Proceedings of the International Absorption Heat Pump Conference, Munich, 1999, pp. 359–366.
[10] J.K. Min, D.H. Choi, Analysis of the absorption process on a horizontal tube using Navier–Stokes equations with surface-tension effects, International Journal of Heat and Mass Transfer 42 (24) (1999) 4567–4578.
[11] C.W. Hirt, B.D. Nichols, Volume of fluid (VOF) method for the dynamics of free boundaries, Journal of Computational Physics 39 (1981) 201–225.
[12] J.U. Brackbill, D.B. Kothe, C. Zemach, A continuum method for modelling surface tension, Journal of Computational Physics 100 (1992) 335–354.
[13] S. Patankar, Numerical heat transfer and fluid flow, McGraw-Hill, 1980.
[14] J. Castro, L. Leal, M. Soria, A. Oliva, Calculation of enhanced water vapour absorption in falling films of LiBr aqueous solutions using the domain decomposition method, in: Proceedings of the European Congress on Computational Methods in Applied Sciences and Engineering (ECCOMAS), volume in CD format, Barcelona, 2000.
[15] Ashrae, ASHRAE HANDBOOK Fundamentals, 1997.
[16] K.M. Kelkar, S.V. Patankar, Numerical method for the prediction of free surface flows in domains with moving boundaries, Numerical Heat Transfer, Part B 31 (1997) 387–399.

[17] D.B. Kothe, R.C. Mjolsness, RIPPLE: a new model for incompressible flows with free surfaces, AIAA journal 30 (11) (1992) 2694–2700.
[18] G.P. Sasmal, J.I. Hochstein, Marangoni convection with a curved and deforming free surface in a cavity, Journal of Fluids Engineering 116 (1994) 577–582.
[19] K.J. Kim, N.S. Berman, B.D. Wood, Surface tension of aqueous lithium bromide+2-ethyl-1-hexanol, Journal of Chemical Engineering Data (39) (1994) 122–124.
[20] M.S. Koenig, G. Grossman, K. Gommed, The role of surfactant adsorption rate in heat and mass transfer enhancement in absorption heat pumps, International Journal of Refrigeration 26 (2003) 129–139.
[21] S. Kulankara, K.E. Herold, Surface tension of aqueous lithium bromide with heat/mass transfer enhancement additives: the effect of additive vapor transport, International Journal of Refrigeration 25 (2002) 383–389.